
Explainable Learning: Implicit Generative Modelling during Training for Adversarial Robustness

Priyadarshini Panda*, and Kaushik Roy

School of Electrical & Computer Engineering, Purdue University, West Lafayette, USA

*pandap@purdue.edu

Abstract

We introduce *Explainable Learning*, *ExL*, an approach for training neural networks that are intrinsically robust to adversarial attacks. We find that the implicit generative modelling of random noise, during posterior maximization, improves a model’s understanding of the data manifold furthering adversarial robustness. We prove our approach’s efficacy and provide a simplistic visualization tool for understanding adversarial data, using Principal Component Analysis. Our analysis reveals that adversarial robustness, in general, manifests in models with higher variance along the high-ranked principal components. We show that models learnt with ExL perform remarkably well against a wide-range of black-box attacks.

1 Introduction

Despite surpassing human performance on several perception tasks, Machine Learning (ML) models remain vulnerable to *adversarial examples*: slightly perturbed inputs that are specifically designed to fool a model during test time [1–4]. Recent works have demonstrated the security danger adversarial attacks pose across several platforms with ML backend such as computer vision [2, 3, 5–7], malware detectors [8–11] and gaming environments [12, 13]. Even worse, adversarial inputs *transfer* across models: same inputs are misclassified by different models trained for the same task, thus enabling simple *Black-Box* (BB)¹ attacks against deployed ML systems [14, 7].

Several works [15–17] demonstrating improved adversarial robustness have been shown to fail against stronger attacks [18]. The state-of-the-art approach for BB defense is ensemble adversarial training that augments the training dataset of the target model with adversarial examples transferred from other pre-trained models [19, 6]. The authors in [20] showed that models can even be made robust to *White-Box* (WB)¹ attacks by closely maximizing the model’s loss with adversarial training. Despite this progress, errors still appear for perturbations beyond what the model is adversarially trained for [21].

There have been several hypotheses explaining the susceptibility of ML models to such attacks. The most common one suggests that the overly linear behavior of deep neural models in a high dimensional input space causes adversarial examples [3, 22]. Another hypothesis suggests that adversarial examples are off the data manifold [23–25]. Combining the two, we infer that excessive linearity causes models to extrapolate their behavior beyond the data manifold yielding pathological results for slightly perturbed inputs. A question worth asking here is: *Can we improve the viability of the model to generalize better on such out-of-sample data?*

In this paper, we propose *Explainable Learning* (*ExL*), wherein we introduce multiplicative noise into the training inputs and optimize it with Stochastic Gradient Descent (SGD) while minimizing the overall cost function over the training data. Essentially, the input noise (randomly initialized at the beginning) is gradually learnt during the training procedure. As a result, the noise approximately

¹BB (WB): attacker has no (full) knowledge of the target model parameters

models the input distribution to effectively maximize the likelihood of the class labels given the inputs. Fig. 1 (a) shows the input noise learnt during different stages of training by a simple convolutional network (*ConvNet2* architecture discussed in Section 3 below), learning handwritten digits from MNIST dataset [26]. We observe that the noise gradually transforms and finally assumes a shape that highlights the most dominant features in the MNIST training data. For instance, the MNIST images are centered digits on a black background. Noise, in fact, learnt this centered characteristic. This suggests that the model not only finds the *right prediction* but also the *right explanation*. Noise inculcates this explainable behavior by discovering some knowledge about the input/output distribution during training.

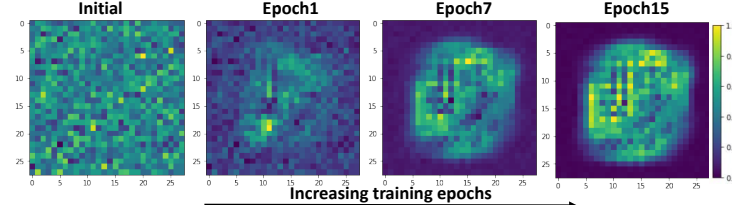


Figure 1: Noise learnt with ExL on MNIST data with mini-batch size =64. The template shown is the mean across all 64 noise templates.

A recent theory [27] suggests that adversarial examples (off manifold misclassified points) occur in close proximity to randomly chosen inputs on the data manifold that are, in fact, correctly classified. With ExL, we hypothesize that the model learns to look in the vicinity of the on-manifold data points and thereby incorporate more out-of-sample data (without using any direct data augmentation) that, in turn, improves its’ generalization capability in the off-manifold input space. We empirically evaluate this hypothesis by visualizing and studying the relationship between the adversarial and the clean inputs using Principal Component Analysis (PCA). Examining the intermediate layer’s output, we discover that models learnt with ExL yield significantly lower distance between adversarial and clean inputs in the Principal Component (PC) subspace, than standard SGD trained models. We further harness this result to establish that ExL noise, indeed, acquires an improved realization of the input/output distribution characteristics that enables it to generalize better. To further substantiate our hypothesis, we also show that ExL globally reduces the dimensionality of the space of adversarial examples [28]. We evaluate our approach on classification tasks such as MNIST, CIFAR10 and CIFAR100 [29] and show that models trained with ExL are extensively more adversarially robust. We also show that combining ExL with ensemble adversarial training significantly extends the robustness of a model, even beyond what it is adversarially trained for.

2 Explainable Learning

2.1 Approach

The basic idea of ExL is to inject random noise with the training data, continually minimizing the overall loss function by learning the parameters, as well as the noise at every step of training. The noise, N , dimensionality is same as the input, X , that is, for a $32 \times 32 \times 3$ sized image, the noise is $32 \times 32 \times 3$. In all our experiments, we use mini-batch SGD optimization. Let’s assume the size of the training minibatch is m and the number of images in the minibatch is k , then, total training images are $m \times k$. Now, the total number of noisy templates are equal to the total number of inputs in each minibatch, k . Since, we want to learn the noise, we use the same k noise templates across all mini-batches 1, 2, ..., m . This ensures that the noise templates inherit characteristics from the entire training dataset. Algorithm 1 shows the training procedure.

It is evident from Algorithm 1 that noise learning at every training step follows the overall loss (\mathcal{L} , say cross-entropy) minimization that in turn enforces the maximum likelihood of the posterior. We found multiplicative noise ($X \times N$) tends to learn improved input characteristics by the end of training. Additive noise ($X + N$), on the other hand, has a disruptive effect that leads to considerable loss in accuracy [Supplementary Fig. S1]. Furthermore, we observe that using only negative gradients (i.e. $\nabla_N \mathcal{L} \leq 0$) during backpropagation for noise modelling yields minimal loss in accuracy as compared to a model trained without any noise [Supplementary Fig. S2]. Next, we present a general optimization perspective considering the maximum likelihood criterion for a classification task to explain adversarial robustness. This will capture the essence of our proposed approach. It is worth

Algorithm 1 Explainable Learning of a model f with parameters θ , Loss Function \mathcal{L} .

Input: Input image X , Target label Y , Noise N , Learning rates η, η_{noise}

Output: Learnt noise N and parameters θ .

```
1: Randomly initialize the parameters  $\theta$  and Noise  $N : \{N^1, \dots, N^k\}$ .
2: repeat
3:   for each minibatch  $\{X^{[1]}, \dots, X^{[m]}\}$  do
4:     Input  $X = \{X^1, \dots, X^k\}$ 
5:     New input  $X' = \{X^1 \times N^1, \dots, X^k \times N^k\}$ 
6:     Forward Propagation:  $\hat{Y} = f(X'; \theta)$ 
7:     Compute loss function:  $\mathcal{L}(\hat{Y}, Y)$ 
8:     Backward Propagation:  $\theta = \theta - \eta \nabla_{\theta} \mathcal{L}; N = N - \eta_{noise} \nabla_N \mathcal{L}$ 
9:   end for
10:  until training converges
```

mentioning that while Algorithm 1 describes the backpropagation step simply by using gradient updates, we can use other techniques like regularization, momentum etc. for improved optimization.

In all our experiments, we initialize the noise N from a random uniform distribution in the range $[0.8, 1]$. We select a high range in the beginning of training to limit the corruption induced on the training data due to the additional noise. During evaluation/testing, we take the mean of the learnt noise across all the templates $((\sum_{i=1}^k N_i)/k)$, multiply the averaged noise with each test image and feed it to the network to obtain the final prediction.

2.2 Adversarial Robustness from Likelihood Perspective

Given a data distribution D with inputs $X \in \mathbb{R}^d$ and corresponding labels Y , a classification/discriminative algorithm models the conditional distribution $p(Y|X; \theta)$ by learning the parameters θ . Since X inherits only the on-manifold data points, a standard model thereby becomes susceptible to adversarial attacks. For adversarial robustness, inclusion of the off-manifold data points while modelling the conditional probability is imperative. An adversarially robust model should, thus, model $p(Y|X, \mathbb{A}; \theta)$, where \mathbb{A} represents the adversarial inputs. Using Bayes rule, we can derive the prediction obtained from posterior modelling from a generative standpoint as:

$$\underset{Y}{\operatorname{argmax}} p(Y|X, \mathbb{A}) = \underset{Y}{\operatorname{argmax}} \frac{p(\mathbb{A}|X, Y)p(X, Y)}{p(X, \mathbb{A})} = \underset{Y}{\operatorname{argmax}} p(\mathbb{A}|X, Y)p(X|Y)p(Y) \quad (1)$$

The methods employing adversarial training [19, 6, 20] directly follow the left-hand side of Eqn. 1 wherein the training data is augmented with adversarial samples ($A \in \mathbb{A}$). Such methods showcase adversarial robustness against a particular form of adversary (e.g. ℓ_{∞} -norm bounded) and hence remain vulnerable to stronger attack scenarios. In an ideal case, A must encompass all set of adversarial examples (or the entire space of off-manifold data) for a concrete guarantee of robustness. However, it is infeasible to anticipate all forms of adversarial attacks during training. From a generative viewpoint (right-hand side of Eqn. 1), adversarial robustness requires modelling of the adversarial distribution while realizing the joint input/output distribution characteristics ($p(X|Y), p(Y)$). Yet, it remains a difficult engineering challenge to create rich generative models that can capture these distributions accurately. Some recent works leveraging a generative model for robustness use a PixelCNN model [24] to detect adversarial examples, or use Generative Adversarial Networks (GANs) to generate adversarial examples [30]. But, one might come across practical difficulties while implementing such methods due to the inherent training difficulty.

With Explainable Learning, we partially address the above difficulty by modelling the noise based on the prediction loss of the posterior distribution. First, let us assume that the noise (\mathbb{N}) introduced with ExL spans a subspace of potential adversarial examples ($\mathbb{N} \subseteq \mathbb{A}$). Based on Eqn. 1 the posterior optimization criterion with the explainable noise (\mathbb{N}) becomes $\underset{Y}{\operatorname{argmax}} p(Y|X, \mathbb{N}) = \underset{Y}{\operatorname{argmax}} p(\mathbb{N}|X, Y)p(X|Y)p(Y)$. The noise learning in ExL (Algorithm 1) indicates an implicit generative modelling behavior, that is constrained towards maximizing $p(\mathbb{N}|X, Y)$ while increasing the likelihood of the posterior $p(Y|X, \mathbb{N})$. We believe that this partial and implicit generative modelling perspective with posterior maximization, during training, imparts an ExL model more knowledge about the data manifold, rendering it less susceptible toward adversarial attacks.

Intuitively, we can justify this robustness in two ways: First, by integrating noise during training, we allow a model to explore multiple directions within the vicinity of the data point (thereby

incorporating more off-manifold data) and hence inculcate that knowledge in its underlying behavior. Second, we note that explainable noise inherits the input data characteristics (i.e. $\mathbb{N} \subset X$) and that the noise-modelling direction ($\nabla_N \mathcal{L}$) is aligned with the loss gradient (that is also used to calculate the adversarial inputs), $\nabla_X \mathcal{L}$. This ensures that the exploration direction coincides with certain adversarial directions improving the model’s generalization capability in such spaces. Next, we empirically demonstrate using PCA that, noise modelling indeed embraces some off-manifold data points. Note, for fully guaranteed adversarial robustness as per Eqn. 1, the joint input/output distribution ($p(X|Y), p(Y)$) has to be realized in addition to the noise modelling and \mathbb{N} should span the entire space of adversarial/off-manifold data.

2.3 PC Subspace Analysis for Explainability & Visualization

PCA serves as a method to reduce a complex dataset to lower dimensions to reveal sometimes hidden, simplified structure that often underlie it. Since the learned representations of a deep learning model lie in a high dimensional geometry of the data manifold, we opted to reduce the dimensionality of the feature space and visualize the relationship between the adversarial and clean inputs in this reduced PC subspace. Essentially, we find the principal components (or eigen-vectors) of the activations of an intermediate layer of a trained model and project the learnt features onto the PC space. To do this, we center the learned features about zero (\mathcal{F}), factorize \mathcal{F} using Singular Value Decomposition (SVD), i.e. $\mathcal{F} = USV^T$ and then transform the feature samples \mathcal{F} onto the new subspace by computing $\mathcal{F}V = US \equiv \mathcal{F}^{PC}$. In Fig. 2 (a), we visualize the learnt representations of the *Conv1 layer* of a ResNet-18 model [31] trained on CIFAR-10 (with standard SGD) along different 2D-projections of the PC subspace in response to adversarial/clean input images. Interestingly, we see that the model’s perception of both the adversarial and clean inputs along high-rank PCs (say, PC1- PC10 that account for maximum variance in the data) is alike. As we move toward lower-rank dimensions, the adversarial and clean image representations dissociate. This implies that adversarial images place strong emphasis on PCs that account for little variance in the data. While we note a similar trend with ExL (Fig. 2 (b)), the dissociation occurs at latter PC dimensions compared to Fig. 2 (a). A noteworthy observation here is that, adversarial examples lie in close vicinity of the clean inputs for both ExL/SGD scenarios ascertaining former theories of [27].

To quantify the dissociation of the adversarial and clean projections in the PC subspace, we calculate the cosine distance ($\mathcal{D}^{PC} = \frac{1}{N} \sum_{i=1}^N 1 - \frac{\mathcal{F}_{clean_i}^{PC} \cdot \mathcal{F}_{adv_i}^{PC}}{\|\mathcal{F}_{clean_i}^{PC}\|_2 \|\mathcal{F}_{adv_i}^{PC}\|_2}$) between them along different PC dimensions. Here, N represents the total number of sample images used to perform PCA and $\mathcal{F}_{clean}^{PC}(\mathcal{F}_{adv}^{PC})$ denote the transformed learnt representations corresponding to clean (adversarial) input, respectively. The distance between the learnt representations (for the *Conv1 layer* of ResNet-18 model from the above scenario) consistently increases for latter PCs as shown in Fig. 2 (c). Interestingly, the cosine distance between adversarial and clean features measured for a model trained with ExL noise is significantly lesser than a standard SGD trained model. This indicates that noise enables the model to look in the vicinity of the original data point and inculcate more adversarial data into its underlying representation. Note, we consider projection across all former dimensions (say, PC0, PC1,...PC100) to calculate the distance at a later dimension (say, PC100) i.e., \mathcal{D}^{PC}_{100} is calculated by taking the dot product between two 100-dimensional vectors: $\mathcal{F}_{clean}^{PC}, \mathcal{F}_{adv}^{PC}$.

To further understand the role of ExL noise in a model’s behavior, we analyzed the variance captured in the *Conv1 layer*’s activations of the ResNet-18 model (in response to clean inputs) by different PCs, as illustrated Fig. 2 (d). If $s_j, j = \{1, \dots, M\}$ are the singular values of the matrix S , the variance along a particular dimension PC_k is defined as: $Var_k = 100 \times (\sum_{i=0}^k s_i^2 / \sum_{i=0}^M s_i^2)$. Var_k along different PCs provides a good measure of how much a particular dimension explains about the data. We observe that ExL noise increases the explainability (or variance) along the high rank PCs, for instance, the net variance obtained from PC0-PC100 with ExL Noise (90%) is more than that of standard SGD (76%). In fact, we observe a similar increase in variance in the leading PC dimensions for other intermediate blocks’ learnt activations of the ResNet-18 model [Supplementary Fig. S3]. We can infer that the increase in variance along the high-rank PCs is a consequence of inclusion of more data points during the overall learning process. Conversely, we can also interpret this as ExL noise embracing more off-manifold adversarial points into the overall data manifold that eventually determines the model’s behavior. This can be attributed to the implicit generative modelling with ExL that imparts a model better realization of the on-/off-manifold data. It is worth mentioning that the variance analysis of the model’s behavior in response to adversarial inputs yields nearly identical results as Fig. 2 (d) [Supplementary Fig. S4].

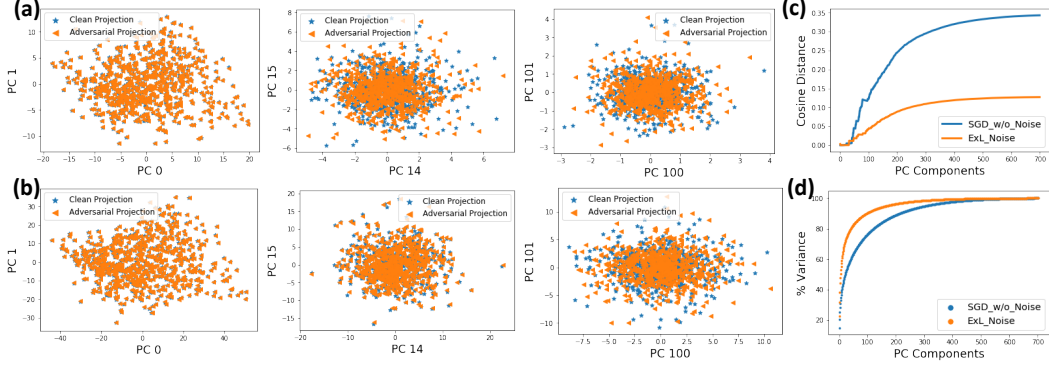


Figure 2: Relationship between the model’s understanding of adversarial and clean inputs in PC subspace when trained with (a) SGD (b) ExL. (c) Cosine Distance between the model’s response to clean and adversarial inputs in the PC subspace. (d) Variance of the *Conv1* layer of ResNet-18 model. (c), (d) compare the SGD/ ExL training scenarios.

Interestingly, the authors in [32] conducted PCA whitening of the raw image data for clean and adversarial inputs and demonstrated that adversarial image coefficients for later PCs have greater variance. Our results from PC subspace analysis corroborates their experiments and further enables us to peek into the model’s behavior for adversarial attacks. Note, for all the PCA experiments above, we used 700 random images sampled from the CIFAR-10 test data, i.e. $N = 700$. In addition, we used the Fast Gradient Sign Method (FGSM) method [3] to create BB adversaries with a step size of $8/255$, from a different source model (ResNet-18 trained with standard SGD). Next, we describe the different attack methods used in our experiments.

2.4 Attack Methods

Given a test image X , an attack model perturbs the image to yield an adversarial image, $X_{adv} = X + \Delta$, such that a classifier f misclassifies X_{adv} . In this work, we consider ℓ_∞ bounded adversaries studied in earlier works [3, 19, 20], wherein the perturbation ($\|\Delta\|_\infty \leq \epsilon$) is regulated by some parameter ϵ . Also, we study BB attacks that is a more reasonable goal for deployed ML models, although WB defense is a stronger notion (that is the ideal security scenario). We consider four algorithms to generate adversarial examples.

Fast Gradient Sign Method (FGSM): This single-step attack is a simple way to generate malicious perturbations in the direction of the loss gradient $\nabla_X \mathcal{L}(X, Y_{true})$ as: $X_{adv} = X + \epsilon sign(\nabla_X \mathcal{L}(X, Y_{true}))$.

Random Step FGSM (R-FGSM): [19] suggested to prepend single-step attacks with a small random step to escape the non-smooth vicinity of a data point that might degrade attacks based on single-step gradient computation. For parameters ϵ, α ($\alpha = \epsilon/2$), the attack is defined as: $X_{adv} = X' + \epsilon sign(\nabla_X \mathcal{L}(X', Y_{true}))$, where $X' = X + \alpha sign(\mathcal{N}(0^d, I^d))$

Iterative FGSM (I-FGSM): This method iteratively applies FGSM k times with a step size of $\beta \geq \epsilon/k$ and projects each step perturbation to be bounded by ϵ . Following [19], we use two-step iterative FGSM attacks.

Projected Gradient Descent with Carlini-Wagner Hinge Loss (PGD-CW): Similar to I-FGSM, this is a multi-step variant of FGSM used as a threat model in [20]. However, instead of using the loss function used to train the target model, we use the hinge-loss function from [18] that is an efficient optimization objective for iteratively finding adversaries. In our experiments, for PGD-CW attacks, we use a high confidence parameter ($\kappa = 50$) following [20] to design strong BB adversaries.

3 Experiments

We evaluated ExL on three datasets: MNIST, CIFAR10 and CIFAR100. For each dataset, we report the accuracy of the models against BB attacks (crafted from the test data) for 4 training scenarios: a) *ExL* Noise, b) Standard *SGD* (without noise), c) *ExL* Noise with Ensemble Adversarial (*EnsAdv*) Training (*ExL_{ens}*), d) *SGD* with *EnsAdv* Training (*SGD_{ens}*). In case of *EnsAdv* training, we augmented the training dataset of the target model with adversarial examples (generated using FGSM), from an independently trained model, with same architecture as the target model. All

networks were trained with mini-batch SGD using a batch size of 64 and momentum of 0.9 (0.5) for CIFAR (MNIST), respectively. For CIFAR10, CIFAR100 we used additional weight decay regularization, $\lambda = 5e - 4$. Note, for noise modelling, we simply used the negative loss gradients ($\nabla_N \mathcal{L} \leq 0$) without additional optimization terms. In general, ExL requires slightly more epochs of training to converge to similar accuracy as standard SGD, a result of the additional input noise modelling. Also, ExL models, if not tuned with proper learning rate, have a tendency to overfit. Hence, the learning rate for noise (η_{noise}) was kept 1-2 orders of magnitude lesser than the overall network learning rate (η) throughout the training process. All networks were implemented in PyTorch²

MNIST: For MNIST, we consider a simple network with 2 Convolutional (C) layers with 32, 64 filters, each followed by 2×2 Max-pooling (M), and finally a Fully-Connected (FC) layer of size 1024, as the target model (ConvNet1: 32C-M-64C-M-1024FC). We trained 4 ConvNet1 models independently corresponding to the different scenarios mentioned above. The EnsAdv (ExL_{ens}, SGD_{ens}) models were trained with BB adversaries created from a separate SGD-trained ConvNet1 model using FGSM with $\epsilon = 0.1$. Table 1 (Columns 3 - 6) illustrates our results for BB attacks crafted from another model (ConvNet2: 10C-M-20C-M-320FC) trained with standard SGD ($ConvNet2_{SGD}$), under different perturbations (ϵ). ExL noise considerably improves the robustness of a model toward BB attacks. Integrating EnsAdv training with ExL further accentuates this robustness. An interesting observation here is that for $\epsilon = 0.1$ (that was the perturbation size for EnsAdv training), both ExL_{ens}/SGD_{ens} yield nearly similar accuracy, $\sim 98\%$. However, for larger perturbation size $\epsilon = 0.2$, the network adversarially trained with ExL noise shows higher prediction capability ($\sim > 2\%$) across all attack methods. The last column of Table 1 gives the worst-case accuracy over all the BB attack methods when the source model is trained with ExL noise ($ConvNet2_{ExL}$). The higher accuracies indicate that ExL models *transfer* attacks at lower rates. As a result, in the remainder of the paper, we conduct BB attacks from SGD trained models to evaluate the adversarial robustness. Note, for PGD-CW attack, we used a step-size of 0.01 over 40 steps to create adversaries bounded by $\epsilon = 0.1/0.2$.

Table 1: **MNIST Accuracy (in %) of ConvNet1 target model for different scenarios.** $\epsilon = 0.1$ for ExL, SGD , $\epsilon = 0.1/0.2$ for ExL_{ens}, SGD_{ens} . Most successful attacks have been marked in bold.

Scenario	Clean	FGSM	R-FGSM (source: $ConvNet2_{SGD}$)	I-FGSM	PGD-CW	Min. BB (source: $ConvNet2_{ExL}$)
<i>SGD</i>	99.1	80	79.2	78	75.1	85
<i>ExL</i>	99.2	83.7	83.1	82	79	81
<i>SGD_{ens}</i>	99	98.2/91	98.1/90.9	98.2/90.8	97.8/89.4	-
<i>ExL_{ens}</i>	99.1	98.6/92.2	98.6/92.7	98.7/93.2	98.4/91.2	-

Table 2: **CIFAR10/ CIFAR100 Accuracy (in %) of ResNet18/ ResNext-29 target model for different scenarios.** $\epsilon = \frac{8}{255} / \frac{16}{255} / \frac{32}{255}$ for $ExL, SGD, ExL_{ens}, SGD_{ens}$. Most successful attacks are marked in bold.

Model	Scenario	Clean	FGSM	R-FGSM	I-FGSM	PGD-CW
ResNet18	<i>SGD</i>	88.8	65.3/58/50.2	65.1/56.4/43.5	50.3/31.9/16.2	52.2/79.7/33
	<i>ExL</i>	87.1	80/74.8 /68.2	80.4/74.9/66.4	81/74.9/ 61	80.5/75.7/66.6
	<i>SGD_{ens}</i>	86.3	80.9/75/67.1	80.8/75.1/65.5	82/76.6/63	80.2/74.4/62.6
	<i>ExL_{ens}</i>	86.4	83.1/79.2/72.6	83.2/ 78.9/71.3	83.7/80.4/72.3	83/79.4/71.6
ResNext29	<i>SGD</i>	71	47.8/38.4/26.6	47.4/36.7/22.8	44.2/30.2/16.8	50.9/40.8/26.7
	<i>ExL</i>	69.4	60.3/53.1 /42.5	60.5/54.3/41.9	61/53.9/ 41.1	62.9/58.5/50.1
	<i>SGD_{ens}</i>	69.8	63.6/ 56.9 /45.4	63.6/57.2 /44.4	64.6/57.5/ 43.2	65.4/60.9/50
	<i>ExL_{ens}</i>	67.3	64.4/60/50.8	64.5/60.4/51.2	64.6/61.4/52.2	64.8/62.8/57

CIFAR: For CIFAR10, we examined our approach on the ResNet-18 architecture. We used the ResNext-29($2 \times 64d$) architecture [33] with bottleneck width 64, cardinality 2 for CIFAR100. Similar to MNIST, we trained the target models separately corresponding to each scenario and crafted BB attacks from an independent source model (either ResNet18/ResNext-29) depending upon the target. For EnsAdv training, we used BB adversaries created using FGSM ($\epsilon = 8/255$) from a separate SGD-trained network different from the source/target model. The results appear in Table 2. We observe that *ExL* (80%/60.3% for CIFAR10/100) significantly boosts the robustness of a model

²Supplementary Section B provides a detailed table of different hyperparameters used to train the source and target models in each scenario.

as compared to SGD (50.3%/44.2% for CIFAR10/100). Note, the improvement here is quite large in comparison to MNIST (that shows only 4% increase from SGD to ExL). In fact, the accuracy obtained with ExL alone, is almost comparable to that of a model adversarially trained with SGD (SGD_{ens}). The richness of the data manifold and feature representation space for larger models and complex datasets allows ExL to model better characteristics in the noise causing increased robustness. As a result, even with EnsAdv training, the accuracy of the ExL_{ens} model is considerably more than SGD_{ens} for perturbations ($\epsilon = (16, 32)/255$) greater than what the network is adversarially trained for. The increased susceptibility of SGD_{ens} for larger ϵ establishes that its' capability is limited by the diversity of adversarial examples shown during training. With ExL_{ens} , the noise modelling during EnsAdv training enables a model to look in the vicinity of adversarial data (in addition to clean data) thereby incorporating more off-manifold data points in the model's behavior. Revisiting the earlier likelihood perspective (Eqn. 1), we can infer that the generative modelling aspect of ExL during posterior maximization explores the loss surface in more detail increasing the overall generalizing capability of the network. Here, for PGD-CW attacks, we use 7 steps of size 2 bounded by ϵ . Note, we also evaluated our approach on a VGG-16 [34] architecture for CIFAR10 and obtained similar results [Supplementary Section A]. We also find that ExL_{ens} models are less vulnerable to BB attacks transferred from other EnsAdv trained models and ExL_{ens} transfer attacks at lower rates than SGD_{ens} .

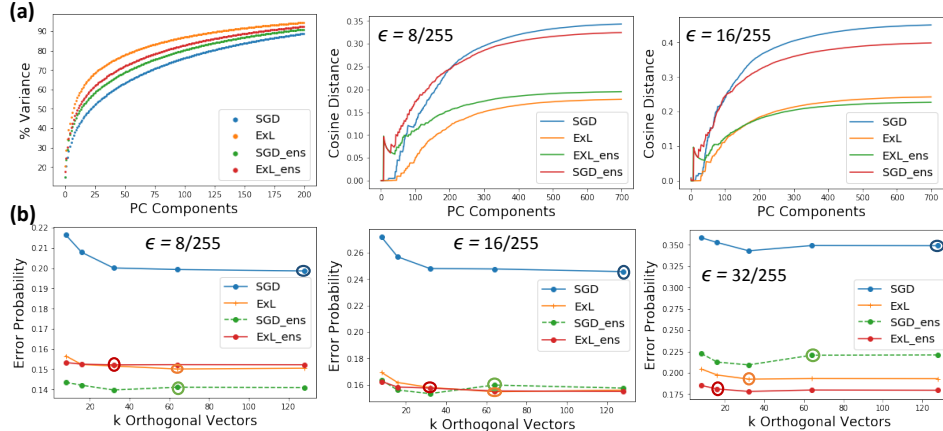


Figure 3: (a) [Left] Variance (in response to clean inputs) across different scenarios for the first 200 PC dimensions. The fact that SGD_{ens} exhibits improved variance than SGD suggests PC variance as a good indicator of adversarial robustness. [Middle, Right] Cosine distance across 700 PCs between clean and adversarial representations for varying ϵ . (b) Adversarial subspace dimensionality for varying ϵ . Largest adversarial dimension with maximum number of misclassified points has been encircled in each scenario.

PC Distance & Variance across different Scenarios : Next, we measured the variance and cosine distance captured by the *Conv1* layer of the ResNet-18 model corresponding to different scenarios (Table 2). Fig. 3 (a) shows that variance across the leading PCs increases in the order $ExL > ExL_{ens} > SGD_{ens} > SGD$. Inclusion of more training data with EnsAdv training informs a model more, leading to improved explainability. We note that while ExL_{ens} yields the maximum accuracy, ExL shows maximum variance of all scenarios. Since we are analyzing only the *Conv1* layer, we get this discrepancy. In Fig. 3 (a), we also plot the cosine distance between the adversarial (created from FGSM with specified ϵ) and clean inputs in the PC subspace. The decreasing distance with EnsAdv training/ ExL with respect to SGD signifies improved realization of the on-/off-manifold data in the model's behavior. Interestingly, for larger perturbation size ($\epsilon = 16/255$), ExL_{ens} has the lowest distance measured across all PC dimensions establishing that integrating ExL with EnsAdv compounds adversarial robustness as compared to standard SGD_{ens} . We get similar trend for $\epsilon = 32/255$. Note, we used a sample set of 700 test images to conduct the PCA.

Adversarial Subspace Dimensionality : To further corroborate that ExL noise embraces adversarial points off the data manifold, we evaluated the adversarial subspace dimension using the Gradient-Aligned Adversarial Subspace (GAAS) method of [28]. We construct k orthogonal vectors $r_1, \dots, r_k \in \{-1, 1\}$ from a regular Hadamard matrix of order $k \in \{2^2, 2^3, \dots, 2^7\}$. We then multiply each r_i component-wise with the gradient, $sign(\nabla_X \mathcal{L}(X, Y_{true}))$. Hence, estimating the dimensionality reduces to finding a set of orthogonal perturbations, r_i with $\|r_i\|_\infty = \epsilon$ in the vicinity of a data point that causes misclassification. For each scenario of Table 2 (CIFAR10 data), we select 350 random

test points, x , and plot the probability that we find at least k orthogonal vectors r_i such that $x + r_i$ is misclassified. Fig. 3 (b) shows the results for varying ϵ . We find that the size of the space of adversarial samples is much lower for a model trained with ExL noise than that of standard SGD. For $\epsilon = 8/255$, we find over 128/64 directions for $\sim 20\%/15\%$ of the points in case of SGD/ExL . With EnsAdv training, the number of adversarial directions for SGD_{ens}/ExL_{ens} reduces to 64/32 that misclassifies $\sim 14/15\%$ of the points. As we increase the perturbation size ($\epsilon = (16, 32)/255$), we observe increasingly reduced number of misclassified points as well as adversarial dimensions for models trained with noise modelling. Explainable learning, thus, yields a small fraction of points near a large adversarial space implying improved robustness.

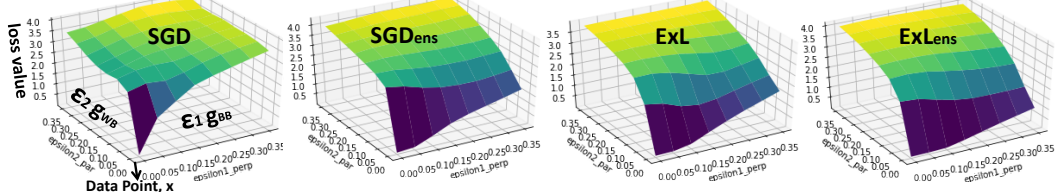


Figure 4: Loss surface of models corresponding to CIFAR10 (Table2). Here, BB and WB gradients are computed with FGSM $\epsilon_{1,2} = 8/255$.

WB Attacks & Loss Surface Smoothening : We find that models trained with ExL noise remain vulnerable to WB attacks. Still, they yield higher WB attack accuracy than standard SGD trained models. For instance, the accuracy of CIFAR10 models of Table 2 $SGD/ExL/SGD_{ens}/ExL_{ens}$ against I-FGSM WB attacks ($\epsilon = 8/255$) is 26/56/19/49%, respectively. Since we did not include any WB perturbations in the training dataset, the EnsAdv trained models yield lower accuracy. Adding the WB adversaries during EnsAdv training increases the accuracy of SGD_{ens}/ExL_{ens} to 59/63%. While adversarial training by inclusion of WB adversaries does improve the robustness of models, noise modelling with ExL furthers this robustness. This is a consequence of the smoothening of the loss surface during noise modelling. We plotted the loss surface of CIFAR10 models on examples $x' = x + \epsilon_1 \cdot g_{BB} + \epsilon_2 \cdot g_{WB}$ in Fig. 4, where g_{BB} is the signed gradient, $sign(\nabla_X \mathcal{L}(X, Y_{true})_{source})$, obtained from the source model (crafting the BB attacks) and g_{WB} is the gradient obtained from the target model itself (crafting WB attacks), $sign(\nabla_X \mathcal{L}(X, Y_{true})_{target})$. We see that the loss surface in case of SGD is highly curved with steep slopes in the vicinity of the data point in both BB and WB direction. The EnsAdv training, SGD_{ens} , smoothes out the slope in the BB direction substantially, justifying their robustness against BB attacks. Models trained with explainable learning (even without any data augmentation) yield a softer loss surface. This is why models trained with explainable noise *transfer* BB attacks at lower rates. The surface in the WB direction along ϵ_2 with ExL, ExL_{ens} still exhibits a sharper curvature (although slightly softer than SGD_{ens}) validating the lower accuracies against WB attacks (compared to BB attacks). As suggested in [19], larger models with additional training on WB perturbations are needed to attain robustness to such attacks.

It is worth mentioning that while we show all our above analysis for CIFAR-10 model, we get similar PCA/ GAAS/ loss surface results for CIFAR100 and MNIST.

4 Conclusion

We proposed *Explainable Learning, ExL*, as a reliable method for adversarial robustness. We used PCA to visualize and quantify a model’s response to adversarial/clean data. While variance and principal subspace analysis help us understand the model’s behavior, we cannot fully describe the structure of the manifold learnt by the linear subspace view. There is a need to combine the behavior of the model across all layers to view the complex optimization landscape learnt by the model. However, PCA does provide a basic intuition about the generalization capability of complex image models. ExL does not change the classification model that makes it easy to be scaled to larger datasets while integrating with other adversarial defense techniques. Empirical results indicate that ExL significantly boosts the robustness of adversarially trained models yielding better results than state-of-the-art techniques [19, 20] (that use adversarial training with MNIST/CIFAR10 data) even for larger perturbation (ϵ) values. Finally, as our likelihood theory indicates, better noise modelling techniques with improved gradient penalties can further improve robustness and requires further investigation. Also, performing noise modelling at intermediate layers to improve explainability and exploring the impact of stronger BB attacks with ExL [14, 35] are other future work directions.

References

- [1] B. Biggio, I. Corona, D. Maiorca, B. Nelson, N. Šrndić, P. Laskov, G. Giacinto, and F. Roli, “Evasion attacks against machine learning at test time,” in *Joint European conference on machine learning and knowledge discovery in databases*. Springer, 2013, pp. 387–402.
- [2] C. Szegedy, W. Zaremba, I. Sutskever, J. Bruna, D. Erhan, I. Goodfellow, and R. Fergus, “Intriguing properties of neural networks,” *arXiv preprint arXiv:1312.6199*, 2013.
- [3] I. J. Goodfellow, J. Shlens, and C. Szegedy, “Explaining and harnessing adversarial examples,” *arXiv preprint arXiv:1412.6572*, 2014.
- [4] N. Papernot, P. McDaniel, S. Jha, M. Fredrikson, Z. B. Celik, and A. Swami, “The limitations of deep learning in adversarial settings,” in *Security and Privacy (EuroS&P), 2016 IEEE European Symposium on*. IEEE, 2016, pp. 372–387.
- [5] S. M. Moosavi Dezfooli, A. Fawzi, and P. Frossard, “Deepfool: a simple and accurate method to fool deep neural networks,” in *Proceedings of 2016 IEEE Conference on Computer Vision and Pattern Recognition (CVPR)*, no. EPFL-CONF-218057, 2016.
- [6] A. Kurakin, I. Goodfellow, and S. Bengio, “Adversarial examples in the physical world,” *arXiv preprint arXiv:1607.02533*, 2016.
- [7] Y. Liu, X. Chen, C. Liu, and D. Song, “Delving into transferable adversarial examples and black-box attacks,” *arXiv preprint arXiv:1611.02770*, 2016.
- [8] P. Laskov *et al.*, “Practical evasion of a learning-based classifier: A case study,” in *Security and Privacy (SP), 2014 IEEE Symposium on*. IEEE, 2014, pp. 197–211.
- [9] W. Xu, Y. Qi, and D. Evans, “Automatically evading classifiers,” in *Proceedings of the 2016 Network and Distributed Systems Symposium*, 2016.
- [10] K. Grosse, N. Papernot, P. Manoharan, M. Backes, and P. McDaniel, “Adversarial perturbations against deep neural networks for malware classification,” *arXiv preprint arXiv:1606.04435*, 2016.
- [11] W. Hu and Y. Tan, “Generating adversarial malware examples for black-box attacks based on gan,” *arXiv preprint arXiv:1702.05983*, 2017.
- [12] S. Huang, N. Papernot, I. Goodfellow, Y. Duan, and P. Abbeel, “Adversarial attacks on neural network policies,” *arXiv preprint arXiv:1702.02284*, 2017.
- [13] V. Behzadan and A. Munir, “Vulnerability of deep reinforcement learning to policy induction attacks,” in *International Conference on Machine Learning and Data Mining in Pattern Recognition*. Springer, 2017, pp. 262–275.
- [14] N. Papernot, P. McDaniel, I. Goodfellow, S. Jha, Z. B. Celik, and A. Swami, “Practical black-box attacks against machine learning,” in *Proceedings of the 2017 ACM on Asia Conference on Computer and Communications Security*. ACM, 2017, pp. 506–519.
- [15] D. Krotov and J. J. Hopfield, “Dense associative memory is robust to adversarial inputs,” *arXiv preprint arXiv:1701.00939*, 2017.
- [16] N. Papernot, P. McDaniel, X. Wu, S. Jha, and A. Swami, “Distillation as a defense to adversarial perturbations against deep neural networks,” in *Security and Privacy (SP), 2016 IEEE Symposium on*. IEEE, 2016, pp. 582–597.
- [17] M. Cisse, P. Bojanowski, E. Grave, Y. Dauphin, and N. Usunier, “Parseval networks: Improving robustness to adversarial examples,” in *International Conference on Machine Learning*, 2017, pp. 854–863.
- [18] N. Carlini and D. Wagner, “Towards evaluating the robustness of neural networks,” in *Security and Privacy (SP), 2017 IEEE Symposium on*. IEEE, 2017, pp. 39–57.

- [19] F. Tramèr, A. Kurakin, N. Papernot, D. Boneh, and P. McDaniel, “Ensemble adversarial training: Attacks and defenses,” *arXiv preprint arXiv:1705.07204*, 2017.
- [20] A. Madry, A. Makelov, L. Schmidt, D. Tsipras, and A. Vladu, “Towards deep learning models resistant to adversarial attacks,” *arXiv preprint arXiv:1706.06083*, 2017.
- [21] Y. Sharma and P.-Y. Chen, “Breaking the madry defense model with l_1 -based adversarial examples,” *arXiv preprint arXiv:1710.10733*, 2017.
- [22] Y. Lou, X. Boix, G. Roig, T. Poggio, and Q. Zhao, “Foveation-based mechanisms alleviate adversarial examples,” Center for Brains, Minds and Machines (CBMM), arXiv, Tech. Rep., 2016.
- [23] I. Goodfellow, Y. Bengio, and A. Courville, “Deep learning.(2016),” *Book in preparation for MIT Press. URL: http://www. deeplearningbook. org*, 2016.
- [24] Y. Song, T. Kim, S. Nowozin, S. Ermon, and N. Kushman, “Pixeldefend: Leveraging generative models to understand and defend against adversarial examples,” *arXiv preprint arXiv:1710.10766*, 2017.
- [25] H. Lee, S. Han, and J. Lee, “Generative adversarial trainer: Defense to adversarial perturbations with gan,” *arXiv preprint arXiv:1705.03387*, 2017.
- [26] Y. LeCun, L. Bottou, Y. Bengio, and P. Haffner, “Gradient-based learning applied to document recognition,” *Proceedings of the IEEE*, vol. 86, no. 11, pp. 2278–2324, 1998.
- [27] J. Gilmer, L. Metz, F. Faghri, S. S. Schoenholz, M. Raghu, M. Wattenberg, and I. Goodfellow, “Adversarial spheres,” *arXiv preprint arXiv:1801.02774*, 2018.
- [28] F. Tramèr, N. Papernot, I. Goodfellow, D. Boneh, and P. McDaniel, “The space of transferable adversarial examples,” *arXiv preprint arXiv:1704.03453*, 2017.
- [29] A. Krizhevsky and G. Hinton, “Learning multiple layers of features from tiny images,” 2009.
- [30] P. Samangouei, M. Kabkab, and R. Chellappa, “Defense-gan: Protecting classifiers against adversarial attacks using generative models,” in *International Conference on Learning Representations*, vol. 9, 2018.
- [31] K. He, X. Zhang, S. Ren, and J. Sun, “Deep residual learning for image recognition,” in *Proceedings of the IEEE conference on computer vision and pattern recognition*, 2016, pp. 770–778.
- [32] D. Hendrycks and K. Gimpel, “Early methods for detecting adversarial images,” 2017.
- [33] S. Xie, R. Girshick, P. Dollár, Z. Tu, and K. He, “Aggregated residual transformations for deep neural networks,” in *Computer Vision and Pattern Recognition (CVPR), 2017 IEEE Conference on*. IEEE, 2017, pp. 5987–5995.
- [34] K. Simonyan and A. Zisserman, “Very deep convolutional networks for large-scale image recognition,” *arXiv preprint arXiv:1409.1556*, 2014.
- [35] S. Baluja and I. Fischer, “Adversarial transformation networks: Learning to generate adversarial examples,” *arXiv preprint arXiv:1703.09387*, 2017.
- [36] “<https://github.com/kuangliu/pytorch-cifar/tree/master/models>.”

SUPPLEMENTARY MATERIAL

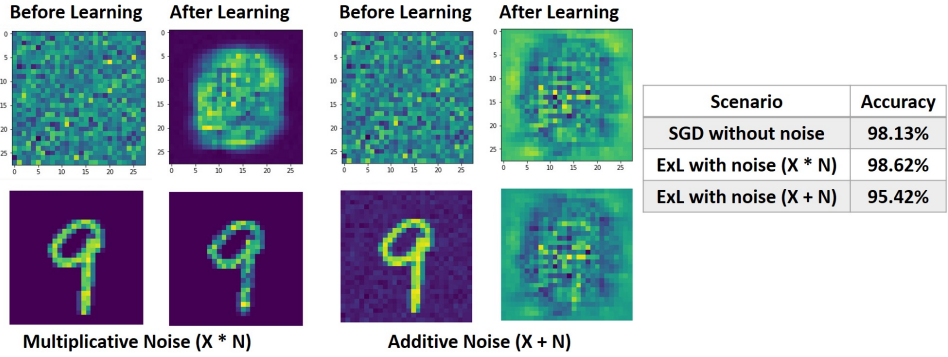


Figure S1: For MNIST dataset, we show the noise template learnt when we use multiplicative/additive noise (N) for Explainable Learning. The final noise-integrated image (for a sample digit ‘9’) that is fed to the network before and after training is also shown. Additive noise disrupts the image drastically. Multiplicative noise, on the other hand, enhances the relevant pixels while eliminating the background. Accuracy corresponding to each scenario is also shown and compared against standard SGD training scenario (without any noise). Here, we train a simple convolutional architecture (ConvNet: 10C-M-20C-M-320FC) of 2 Convolutional (C) layers with 10, 20 filters, each followed by 2×2 Max-pooling (M) and a Fully-Connected (FC) layer of size 320. We use mini-batch SGD with momentum of 0.5, learning rate ($\eta=0.1$) decayed by 0.1 every 15 epochs and batch-size 64 to learn the network parameters. We trained 3 ConvNet models independently corresponding to each scenario for 30 epochs. For the ExL scenarios, we conduct noise modelling with only negative loss gradients ($\nabla \mathcal{L}_N \leq 0$) with noise learning rate, $\eta_{noise} = 0.001$, throughout the training process. Note, the noise image shown is the average across all 64 noise templates.

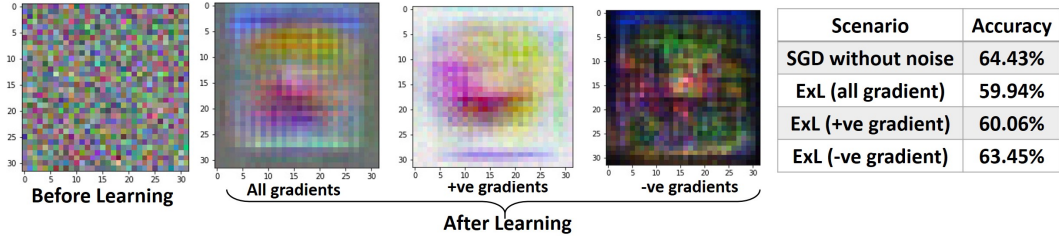


Figure S2: Here, we showcase the noise learnt by a simple convolutional network (ConvNet: 10C-M-20C-M-320FC), learning the CIFAR10 data with ExL (multiplicative noise) under different gradient update conditions. As with MNIST (Fig. S1), we observe that the noise learnt enhances the region of interest while deemphasizing the background pixels. Note, the noise in this case has RGB components as a result of which we see some prominent color blobs in the noise template after training. The performance table shows that using only negative gradients (i.e. $\nabla \mathcal{L}_N \leq 0$) during backpropagation for noise modelling yields minimal loss in accuracy as compared to a standard SGD trained model. We use mini-batch SGD with momentum of 0.9, weight decay 5e-4, learning rate ($\eta=0.01$) decayed by 0.2 every 10 epochs and batch-size 64 to learn the network parameters. We trained 4 ConvNet models independently corresponding to each scenario for 30 epochs. For the ExL scenarios, we conduct noise modelling by backpropagating the corresponding gradient with noise learning rate ($\eta_{noise} = 0.001$) throughout the training process. Note, the noise image shown is the average across all 64 noise templates.

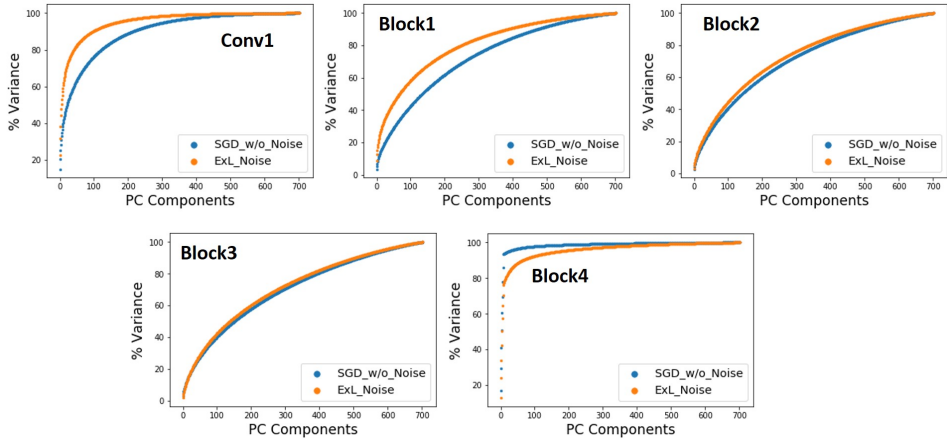


Figure S3: Here, we show the variance captured in the leading Principal Component (PC) dimensions for the initial convolutional layer's (*Conv1*) and intermediate blocks' learnt activations of a ResNet-18 model trained on CIFAR10 data. We compare the variance of the learnt representations (in response to clean inputs) for each block across two scenarios: SGD (without noise) and ExL (with noise). Note, we capture the variance of the final block's activations before average pooling. That is, the activations of *Block4* have dimension $512 \times 4 \times 4$. We observe that ExL noise increases the explainability (or variance) along the high rank PCs. Also, as we go deeper into the network, the absolute difference of the variance values between *SGD/ExL* decreases. This is expected as the contribution of input noise on the overall representations decreases as we go deeper into the network. Moreover, there is a generic-to-specific transition in the hierarchy of learnt features of a deep neural network. Thus, the linear PC subspace analysis to quantify a model's knowledge of the data manifold is more applicable in the earlier layers, since they learn more general input-related characteristics. Nonetheless, we see that ExL model yields widened explainability than *SGD* for each intermediate layer except the final *Block4* that feeds into the output layer. We use mini-batch SGD with momentum of 0.9, weight decay 5e-4, learning rate ($\eta=0.1$) decayed by 0.1 every 30 epochs and batch-size 64 to learn the network parameters. We trained 2 ResNet-18 models independently corresponding to each scenario for 60 epochs. For noise modelling, we use $\eta_{noise} = 0.001$ decayed by 0.1 every 30 epochs. Note, we used a sample set of 700 test images to conduct the PCA.

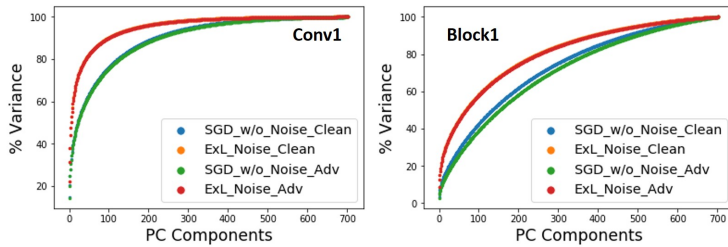


Figure S4: Here, we show the variance captured in the leading Principal Component (PC) dimensions for the *Conv1* and *Block1* learnt activations in response to both clean and adversarial inputs for ResNet-18 models corresponding to the scenarios discussed in Fig. S3. The model's variance for both clean and adversarial inputs are exactly same in case of *ExL/SGD* for *Conv1* layers. For *Block1*, the adversarial input variance is slightly lower in case of *SGD* than that of clean input. With *ExL*, the variance is still the same for *Block1*. This indicates that PC variance statistics cannot differentiate between a model's knowledge of on/off-manifold data. It only tells us whether a model's underlying representation has acquired more knowledge about the data manifold. To analyze a model's understanding of adversarial data, we need to look into the relationship between the clean and adversarial projection onto the PC subspace and measure the cosine distance. Note, we used the Fast Gradient Sign Method (FGSM) method [3] to create BB adversaries with a step size of 8/255, from another independently trained ResNet-18 model (*source*) with standard SGD. The *source* attack model has the same hyperparameters as the *SGD* model in Fig. S3 and is trained for 40 epochs.

Section A: CIFAR10 performance on VGG16 architecture with Explainable Learning

Table S1: **CIFAR10 Accuracy (in %) on VGG16 target model for different scenarios.** $\epsilon = \frac{8}{255} / \frac{16}{255} / \frac{32}{255}$ for $ExL, SGD, ExL_{ens}, SGD_{ens}$. Most successful attacks are marked in bold.

Scenario	Clean	FGSM	R-FGSM	I-FGSM	PGD-CW
<i>SGD</i>	88.6	69.4/61/50.2	70.1/60.3/46	60.3/ 39.5/19.5	57.7/45.5/34.4
<i>ExL</i>	84.5	78.3/73.1/65.2	78.4/73/64.3	77.6/ 69.9/53.5	77/71.9/63.8
<i>SGD_{ens}</i>	86.4	72/63.8/54	71.9/63.5/50.8	66.1/ 46.8/25.7	63.7/52.2/42.2
<i>ExL_{ens}</i>	86.2	82.4/77.9/71.5	82.3/78/71.1	82.4/ 77.6/68.6	81.9/78.8/73.4

Even for VGG16, *ExL* significantly boosts the robustness of a model as compared to *SGD*. In fact, the accuracy obtained with *ExL* alone, is better than that of a model adversarially trained with SGD (*SGD_{ens}*). Furthermore, with Ensemble Adversarial training (EnsAdv), the accuracy of the *ExL_{ens}* model is significantly greater than *SGD_{ens}* for perturbations ($\epsilon = (16, 32)/255$) greater than what the network is adversarially trained for. The richness of the data manifold and feature representation space in case of a large model like VGG16 allows ExL to model better characteristics in the noise causing increased robustness. Note, we trained the target models separately corresponding to each scenario and crafted BB attacks from an independent source VGG16 model. For EnsAdv training, we used black-box adversaries created using FGSM ($\epsilon = 8/255$) from a separate SGD-trained network different from the source/target models.

We use mini-batch SGD with momentum of 0.9, weight decay 5e-4 for training the weight parameters of the VGG16 models. For noise modelling, we use negative loss gradients during backpropagation. A detailed description of the learning rate and epochs is shown in Table S2. The hyperparameters corresponding to each scenario (of Table S1) are shown in Rows 1-4 under *Target* type. The hyperparameters for the source model used to attack the target models is shown in Row 5 under *Source* type. The model used to generate black box adversaries to augment the training dataset of the *SGD_{ens}*, *ExL_{ens}* target models is shown in Row 6 under *EnsAdv* type. Furthermore, in all our experiments, for EnsAdv training (*SGD_{ens}*), we use a slightly different approach than [6]. Instead of using a weighted loss function that controls the relative weight of adversarial/clean examples in the overall loss computation, we use a different learning rate η_{adv}/η ($\eta_{adv} < \eta$) when training with adversarial/clean inputs, respectively, to learn the network parameters. Accordingly, while performing adversarial training with explainable learning (*ExL_{ens}*), the noise modelling learning rate in addition to overall learning rate, η_{adv}/η , for adversarial/clean inputs is also different, $\eta_{noiseadv}/\eta_{noise}$ ($\eta_{noiseadv} < \eta_{noise}$). We also show the test accuracy (on clean data) for each model in Table S2 for reference. Note, the learning rate in each case decays by a factor of 0.1 every 20 epochs (Column 5 in Table S2).

Table S2: **Hyperparameter Table for training VGG16 models on CIFAR10 data**

Model Type	Training Method	Epochs	η/η_{adv}	η, η_{adv} decay/step-size	$\eta_{noise}/\eta_{noiseadv}$	$\eta_{noise}, \eta_{noiseadv}$ decay/step-size	Test Accuracy in (%)
Target	<i>SGD</i>	100	0.1/–	0.1/20	–	–	88.6
	<i>ExL</i>	41	0.1/–	0.1/20	0.001/–	0.1/20	84.5
	<i>SGD_{ens}</i>	42	0.1/0.05	0.1/20	–	–	86.4
	<i>ExL_{ens}</i>	42	0.1/0.05	0.1/20	0.001/0.0005	0.1/20	86.2
Source	<i>SGD</i>	61	0.1/–	0.1/20	–	–	89.1
EnsAdv	<i>SGD</i>	41	0.1/–	0.1/20	–	–	87.9

Section B: Hyperparameters for the MNIST/CIFAR10/CIFAR100 experiments

The Pytorch implementation of ResNet-18/VGG16 architecture for CIFAR10 and ResNext-29 architecture for CIFAR100 were taken from [36]. For CIFAR10/CIFAR100, we use mini-batch SGD with momentum of 0.9, weight decay 5e-4 and batch size 64 for training the weight parameters of the models. A detailed description of the learning rate and epochs for ResNet18 model (corresponding to Table 2 in main paper) is shown in Table S3. Similarly, Table S4 shows the parameters for ResNext-29 model. The notations here are similar to that of Table S2.

Table S3: Hyperparameter Table for training ResNet18 models on CIFAR10 data

Model Type	Training Method	Epochs	η/η_{adv}	η, η_{adv} decay/step-size	$\eta_{noise}/\eta_{noise_{adv}}$	$\eta_{noise}, \eta_{noise_{adv}}$ decay/step-size	Test Accuracy in (%)
Target	<i>SGD</i>	120	0.1/–	0.1/30	–	–	88.8
	<i>ExL</i>	120	0.1/–	0.1/30	0.001/–	0.1/30	87.1
	<i>SGD_{ens}</i>	80	0.1/0.05	0.1/30	–	–	86.3
	<i>ExL_{ens}</i>	120	0.1/0.05	0.1/30	0.001/0.0005	0.1/30	86.4
Source	<i>SGD</i>	300	0.1/–	0.1/100	–	–	89
EnsAdv	<i>SGD</i>	31	0.1/–	0.1/30	–	–	81

Table S4: Hyperparameter Table for training ResNext29 models on CIFAR100 data

Model Type	Training Method	Epochs	η/η_{adv}	η, η_{adv} decay/step-size	$\eta_{noise}/\eta_{noise_{adv}}$	$\eta_{noise}, \eta_{noise_{adv}}$ decay/step-size	Test Accuracy in (%)
Target	<i>SGD</i>	100	0.1/–	0.1/40	–	–	71
	<i>ExL</i>	58	0.1/–	0.1/20	0.001/–	0.1/20	69.4
	<i>SGD_{ens}</i>	42	0.1/0.05	0.1/20	–	–	69.8
	<i>ExL_{ens}</i>	48	0.1/0.05	0.1/20	0.001/0.0005	0.1/20	67.3
Source	<i>SGD</i>	34	0.1/–	0.1/10	–	–	67.2
EnsAdv	<i>SGD</i>	45	0.1/–	0.1/20	–	–	71.3

For MNIST, we use 2 different architectures as source/ target models. ConvNet1: 32C-M-64C-M-1024FC is the model used as target. ConvNet2: 10C-M-20C-M-320FC is the model used as source. Here, we use mini-batch SGD with momentum of 0.5, batch size 64, for training the weight parameters. Table S5 shows the hyperparameters used to train the models in Table 1 of main paper. In Table 1 of main paper, we showed the accuracy across different scenarios for BB attacks from a source model trained with ExL noise. Accordingly, in Table S5 we show the training parameters for the ExL trained source attack model.

Table S5: Hyperparameter Table for training ConvNet1/ConvNet2 models on MNIST data

Model Type	Training Method	Epochs	η/η_{adv}	η, η_{adv} decay/step-size	$\eta_{noise}/\eta_{noise_{adv}}$	$\eta_{noise}, \eta_{noise_{adv}}$ decay/step-size	Test Accuracy in (%)
Target	<i>SGD</i>	100	0.01/–	0.1/50	–	–	99.1
	<i>ExL</i>	150	0.01/–	0.1/50	0.001/–	0.1/50	99.2
	<i>SGD_{ens}</i>	64	0.01/0.005	0.1/30	–	–	99
	<i>ExL_{ens}</i>	32	0.01/0.005	0.1/30	0.001/3.3e-5	0.1/30	99.1
Source	<i>SGD</i>	15	0.01/–	–/–	–	–	98.6
ConvNet2	<i>ExL</i>	29	0.01/–	–/–	–	–	98.8
EnsAdv	<i>SGD</i>	15	0.01/–	–/–	–	–	98.8
ConvNet1							